

## Micromachined ultrasonic transducers: 11.4 MHz transmission in air and more

Igal Ladabaum, B. T. KhuriYakub, and Dimitri Spoliansky

Citation: *Appl. Phys. Lett.* **68**, 7 (1996); doi: 10.1063/1.116764

View online: <http://dx.doi.org/10.1063/1.116764>

View Table of Contents: <http://apl.aip.org/resource/1/APPLAB/v68/i1>

Published by the [American Institute of Physics](http://www.aip.org).

---

### Related Articles

Using quantum memory techniques for optical detection of ultrasound

*Appl. Phys. Lett.* **101**, 191112 (2012)

Simultaneous structure and elastic wave velocity measurement of SiO<sub>2</sub> glass at high pressures and high temperatures in a Paris-Edinburgh cell

*Rev. Sci. Instrum.* **83**, 033905 (2012)

Analysis of the particle stability in a new designed ultrasonic levitation device

*Rev. Sci. Instrum.* **82**, 105111 (2011)

Modeling of ultrasound transmission through a solid-liquid interface comprising a network of gas pockets

*J. Appl. Phys.* **110**, 044910 (2011)

Combined ultrasonic elastic wave velocity and microtomography measurements at high pressures

*Rev. Sci. Instrum.* **82**, 023906 (2011)

---

### Additional information on *Appl. Phys. Lett.*

Journal Homepage: <http://apl.aip.org/>

Journal Information: [http://apl.aip.org/about/about\\_the\\_journal](http://apl.aip.org/about/about_the_journal)

Top downloads: [http://apl.aip.org/features/most\\_downloaded](http://apl.aip.org/features/most_downloaded)

Information for Authors: <http://apl.aip.org/authors>

## ADVERTISEMENT

**AIP** | Applied Physics  
Letters

**EXPLORE WHAT'S  
NEW IN APL**

**SUBMIT YOUR PAPER NOW!**

**SURFACES AND INTERFACES**  
Focusing on physical, chemical, biological, structural, optical, magnetic and electrical properties of surfaces and interfaces, and more...

**ENERGY CONVERSION AND STORAGE**  
Focusing on all aspects of static and dynamic energy conversion, energy storage, photovoltaics, solar fuels, batteries, capacitors, thermoelectrics, and more...

# Micromachined ultrasonic transducers: 11.4 MHz transmission in air and more

Igal Ladabaum<sup>a)</sup> and B. T. Khuri-Yakub  
*E. L. Ginzton Laboratory, Stanford University, Stanford, California 94305*

Dimitri Spoliansky  
*Ecole Normale Supérieure, 45 Rue D'Ulm, 75005 Paris, France*

(Received 28 July 1995; accepted for publication 26 October 1995)

The fabrication and modeling of novel, capacitive, ultrasonic air transducers is reported. Transmission experiments in air at 11.4, 9.2, and 3.1 MHz are shown to correspond with theory. The transducers are made using surface micromachining techniques, which enable the realization of center frequencies ranging from 1.8 to 11.6 MHz. The bandwidth of the transducers ranges from 5% to 20%, depending on processing parameters. Custom circuitry is able to detect 10 MHz capacitance fluctuations as small as  $10^{-18}$  F, which correspond to displacements on the order of  $10^{-3}$  Å, in a bandwidth of 2 MHz with a signal to noise ratio of 20 dB. Such detection sensitivity is shown to yield air transducer systems capable of withstanding over 100 dB of signal attenuation, a figure of merit that has significant implications for ultrasonic imaging, nondestructive evaluation, gas flow and composition measurements, and range sensing. © 1996 American Institute of Physics. [S0003-6951(95)00252-6]

The generation of ultrasound in air is challenging because the acoustic impedance of air ( $400 \text{ kg/m}^2 \text{ s}$ ) is many orders of magnitude smaller than the impedance of piezoelectric materials commonly used to excite ultrasonic vibrations ( $\sim 30 \times 10^6 \text{ kg/m}^2 \text{ s}$ ). The large impedance mismatch implies that piezoelectric air transducers are inherently inefficient. In order to improve efficiency, a matching layer is usually placed in between the piezoelectric and the air. The matching layer solution is problematic for three reasons. First, the impedance mismatch is so large that matching layer materials with the necessary characteristic impedance are rarely available. Second, the improved energy coupling comes at the expense of bandwidth. Third, high frequency transducers require impractically thin matching layers. Attempts to maximize the energy transfer from the piezoelectric element to the air and vice versa have achieved moderate success.<sup>1-3</sup> However, the increased complexity of the more efficient devices reduces their reliability and increases their cost.

Transducers based on a different principle of actuation and detection offer more promise than optimized piezoelectric transducers. In this letter, we report the fabrication and modeling of capacitive micromachined ultrasonic transducers (MUTs). Although magnetoacoustic and capacitive devices have been reported,<sup>4-8</sup> our transducer system is the first to demonstrate 11.4 MHz transmission in air. Furthermore, we present a simplified theoretical model which accounts for the behavior observed.

The MUT consists of circular silicon nitride membranes suspended above heavily doped silicon bulk (Fig. 1). When a voltage is applied between the membrane and the bulk, electrostatic forces attract the membrane toward the bulk and stress forces within the membrane resist the attraction. If the membrane is driven by an alternating voltage at its mechani-

cal resonance frequency, large displacements, and consequently significant sound generation, will result. Conversely, if the membrane is biased appropriately and subjected to ultrasonic waves at resonant frequencies, significant detection currents will be generated. Micromachining is the chosen vehicle for device fabrication because the membrane's dimensions (microns) and residual stress (hundreds of MPa's) can be tailored to yield mechanical resonance frequencies in the MHz range. Silicon and silicon nitride have excellent mechanical properties, and can be readily patterned using the wide repertoire of procedures invented by the semiconductor industry.

The fabrication sequence is simple (Fig. 2). A highly doped, *p*-type  $\langle 100 \rangle$  4 in. silicon wafer is cleaned and a  $1 \mu\text{m}$  oxide layer is grown with a wet oxidation process. A 5000 Å layer of LPCVD nitride is then deposited. The residual stress of the nitride can be varied by changing the proportion of silane to ammonia during the deposition process. After the backside of the wafer is stripped, a chrome adhesion layer and a 500 Å film of gold are evaporated onto both sides of the wafer. A pattern of etchant holes is then transferred to the wafer lithographically, followed by a gold and nitride etch. Thus, access holes are generated through which HF can subsequently attach the sacrificial oxide layer. The etch time determines the dimensions of the membrane. One transducer

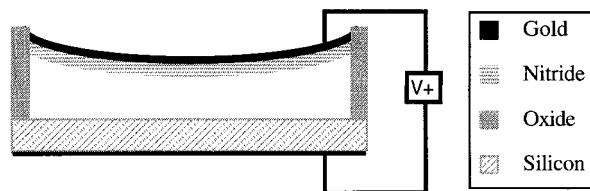


FIG. 1. Schematic of one element of a MUT.

<sup>a)</sup>Electronic mail: igal@leland.stanford.edu

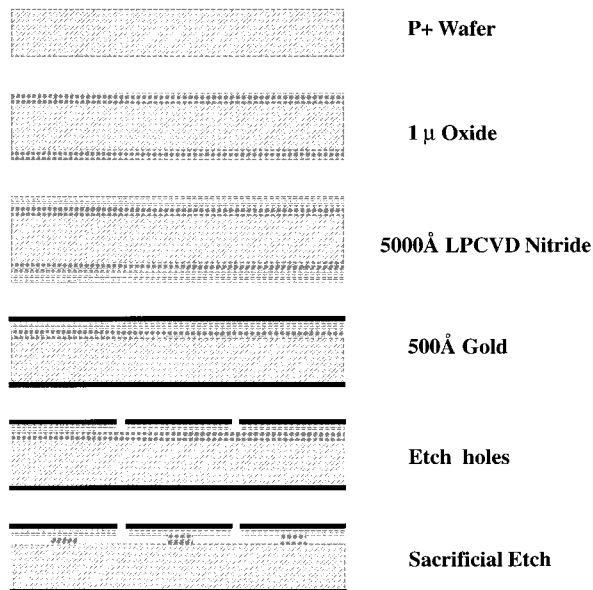


FIG. 2. Overview of process for MUT fabrication.

consists of a matrix of individual elements with a spacing of 25, 50, or 100  $\mu\text{m}$ .

The theoretical model accounts for both the static and dynamic behavior of the device. The static analysis allows an understanding of the operating point about which the dynamic analysis applies. Because the electrostatic attraction force varies as the square of the electrode separation, while the restoring force varies approximately linearly, certain voltages and separations lead to membrane collapse. Furthermore, the behavior is hysteretic; after collapse, the membrane requires a fairly low voltage condition to snap back. The static analysis begins with the general plate equation:<sup>9</sup>

$$\frac{(Y_0 + A\sigma)t_m^3}{12(1-\nu^2)} \nabla^4 x - \sigma t_m \nabla^2 x - P_E(r) = 0, \quad (1)$$

where  $Y_0$  is Young's modulus,  $A$  is area,  $\sigma$  is residual stress,  $t_m$  is the membrane thickness,  $\nu$  is Poisson's ratio,  $x$  is membrane displacement, and  $P_E(r)$  is the electrostatic pressure as a function of radius. Neglecting bending stresses and introducing polar coordinates yields the membrane equation:

$$\sigma t_m \left( \frac{d^2 x}{dr^2} + \frac{1}{r} \frac{dx}{dr} \right) + P_E(r) = 0. \quad (2)$$

The Green function for this equation is

$$G(r, \xi) = \begin{cases} \xi \ln(\xi) \rightarrow 0 < \frac{r}{a} < \xi < 1 \\ \xi \ln\left(\frac{r}{a}\right) \rightarrow 0 < \xi < \frac{r}{a} < 1 \end{cases} \quad (3)$$

where  $a$  is the membrane radius and  $\xi$  is a variable of integration. The solution for the displacement as a function of radius then becomes

$$\frac{a^2}{\sigma t_m} \int_0^1 G(r, \xi) P_E(\xi) d\xi, \quad (4)$$

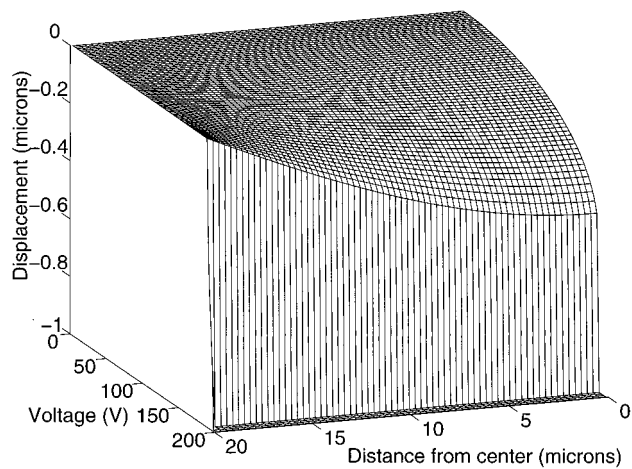


FIG. 3. Membrane displacement as a function of voltage. Note collapse at 190 V. Collapse voltage will vary with membrane properties and device geometry.

which we solve iteratively on a computer (see Figs. 3 and 4).

The dynamic analysis begins by adding the membrane's inertia term to (2):

$$\sigma t_m \left( \frac{d^2 x}{dr^2} + \frac{1}{r} \frac{dx}{dr} \right) + \rho t_m \frac{d^2 x}{dr^2} + P_E(r) = 0, \quad (5)$$

where  $\rho$  is the membrane density. The solution, when taking  $P_E(r) = P_{\text{uniform}}$  and using phasor analysis, is found to be

$$x(r) = \frac{P_{\text{uniform}}}{\omega^2 \rho t_m} \left( \frac{J_0(kr)}{J_0(ka)} - 1 \right), \quad (6)$$

where  $\omega$  is frequency  $k = \omega \sqrt{\rho/\sigma}$  and  $J_0$  is the zeroth order Bessel function. If we define the mechanical impedance of the membrane as the ratio of pressure to average velocity, we obtain

$$Z_m = \frac{P_{\text{uniform}}}{v_{\text{average}}} = \frac{-i\omega \rho t_m k a J_0(ka)}{[2J_1(ka) - ka J_0(ka)]} A. \quad (7)$$

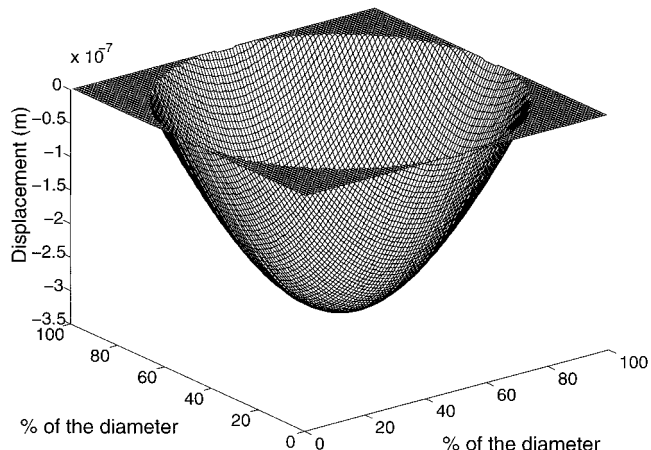


FIG. 4. Calculated membrane shape before collapse.

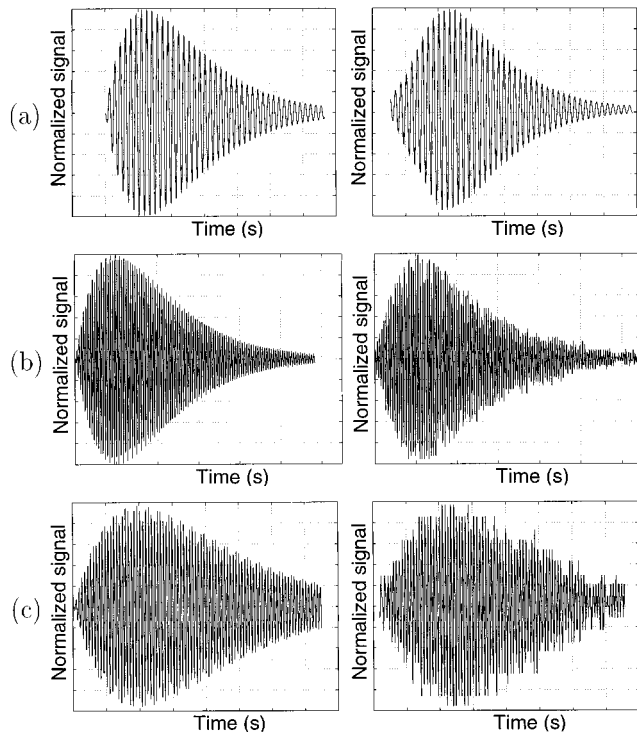


FIG. 5. Received signals of transmission experiments: theory vs experiment. (a) 3.1 MHz (50  $\mu\text{m}$ ), (b) 9.2 MHz (25  $\mu\text{m}$ ), (c) 11.4 MHz (25  $\mu\text{m}$ ).

Equation (7) can be used to derive a two-port model.<sup>9</sup> Computer simulations using the two-port model match the experimental results of transmission, in air, at 11.4, 9.2, and 3.1 MHz (Fig. 5).

The transmission experiments necessitated custom detection circuitry. The custom detection circuitry consists of a transconductance amplifier system used to detect the currents generated by the transducer. A first order analysis yields

$$I = d \frac{(CV)}{dt},$$

which, in phasor form with constant voltage, becomes

$$I = \omega VC.$$

For our circuit, the noise floor is  $2\text{pA}/\sqrt{\text{Hz}}$  as per a circuit simulator, thus, for a 10 MHz transducer with a hypothetical 2 MHz bandwidth operating at a 60 V bias, the noise floor corresponds to a capacitance of  $7.5 \times 10^{-19}$  F. Thus, a 100 pF transducer with a 1  $\mu\text{m}$  gap can detect displacements on the order of  $10^{-3}$  Å with a 20 dB signal to noise ratio. Furthermore, affording a 100 dB signal loss would require emitter displacement on the order of 100 Å. Computer simulations using the two-port model derived from the theory above indicate that such displacements would require a 6 V ac signal riding on 60 V dc. Thus it is clear that these transducers are capable of high power excitation and high sensitivity detection, enabling many applications requiring a large dynamic range.

Impedance spectra of the resonant behavior of two transducers are shown in Fig. 6. For transducers made from inde-

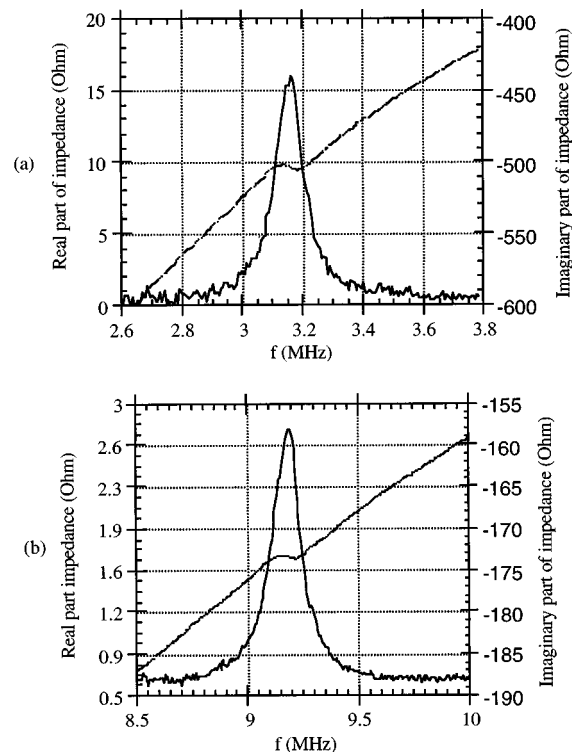


FIG. 6. Electrical impedance of two transducers. (a) 3.1 MHz, (b) 9.2 MHz.

pendent circular elements, the bandwidth is of the order of 5%. For transducers in which an element's etching results in membrane continuity with its neighbors, the bandwidth is measured to be of the order of 20%. Thus, both high efficiency and broad bandwidth can be achieved.

In summary, we have reported the transmissions of 11.4 MHz ultrasound in air. We have described the technology and the theory that govern the behavior of the transducers used in the transmission experiments. We have shown that broadband transducer systems capable of withstanding 100 dB of loss are feasible, an accomplishment that has significant implications in the fields of imaging and nondestructive evaluation.

This work was made possible by a grant from the U. S. Office of Naval Research. We would also like to acknowledge the helpful contributions of Victor Honein and Matt Haller.

<sup>1</sup>L. C. Lynnworth, IEEE Trans. Sonic Ultrason. **SU-12**, 37 (1965).

<sup>2</sup>S. Schiller, C. K. Hsieh, C. H. Chou, and B. T. Khuri-Yakub, Rev. Prog. Quantum Non-Destr. Eval. **9**, 795 (1990).

<sup>3</sup>M. I. Haller and B. T. Khuri-Yakub, Proc. IEEE Ultrason. Symp. 937 (1992).

<sup>4</sup>C. Edwards and S. B. Palmer, IEEE Trans. Magn. **26**, 2080 (1990).

<sup>5</sup>G. M. Sessler, Sens. Actuators A **26**, 323 (1991).

<sup>6</sup>W. Kuhnel and G. Hess, Sens. Actuators A **32**, 560 (1992).

<sup>7</sup>D. W. Schindel and D. A. Hutchins, IEEE Trans. Ultrason. Ferroelectr. Freq. Control **42**, 42 (1995).

<sup>8</sup>M. I. Haller, Doctorate Thesis, Stanford University, 1994.

<sup>9</sup>W. P. Mason, *Electromechanical Transducers and Wave Filters* (Van Nostrand, New York, 1942).